Cerebral Cortex, April 2018;28: 1358–1368

doi: 10.1093/cercor/bhx062
Advance Access Publication Date: 14 March 2017
Original Article

ORIGINAL ARTICLE

Functional Brain Parcellations of the Infant Brain and the Associated Developmental Trends

Feng Shi[1], Andrew P. Salzwedel[1], Weili Lin[2], John H. Gilmore[3] and Wei Gao[1]

[1]Department of Biomedical Sciences and Imaging, Biomedical Imaging Research Institute (BIRI), Cedars-Sinai Medical Center, Los Angeles, CA 90048, USA, [2]Department of Radiology, Biomedical Research Imaging Center, University of North Carolina at Chapel Hill, Chapel Hill, NC 27599, USA and [3]Department of Psychiatry, University of North Carolina at Chapel Hill, Chapel Hill, NC 27599, USA

Address Correspondence to Wei Gao, Department of Biomedical Sciences and Imaging, Biomedical Imaging Research Institute (BIRI), Cedars-Sinai Medical Center, 8700 Beverly Blvd, PACT800, Los Angeles, CA 90048, USA. Email: wei.gao@cshs.org

Feng Shi and Andrew P. Salzwedel contributed equally to this work.

Abstract

Resting-state functional connectivity studies have dramatically improved our understanding of the early human brain functional development during the past decade. However, one emerging problem that could potentially impede future progresses in the field is the definition of regions of interest (ROI), since it is well known that functional connectivity estimation can be seriously contaminated by within-ROI signal heterogeneity. In this study, based on a large-scale rsfMRI data set in human infants (230 neonates, 143 1-year olds, and 107 2-year olds), we aimed to derive a set of anatomically constrained, infant-specific functional brain parcellations using functional connectivity-based clustering. Our results revealed significantly higher levels of signal homogeneity within the newly defined functional parcellations compared with other schemes. Importantly, the global functional connectivity patterns associated with the newly defined functional subunits demonstrated significantly increasing levels of differentiation with age, confirming increasing levels of local specialization. Subsequent whole brain connectivity analysis revealed intriguing patterns of regional-level functional connectivity developments and system-level hub redistribution during infancy. Overall, the newly derived infant-specific functional brain parcellations and the associated novel developmental patterns will likely prove valuable for future early developmental studies using the functional connectivity technique.

Key words: atlas, connectome, early development, functionally connectivity, graph cut

Introduction

Fostering the most dynamic postnatal brain development (Gilmore et al. 2007, 2012; Gao et al. 2009a, 2011, 2016; Tau and Peterson 2010), the infancy period represents both great opportunity and vulnerability (Singer et al. 2001; Phillips et al. 2005; Karevold et al. 2009). A better understanding of the brain's functional organization during this period is critical for potential early identification of risks for developmental problems (e.g., language delay, learning difficulties) and/or brain disorders (e.g., autism) (Camfield et al. 1996; Burton et al. 2009; Lee et al. 2011; Braakman et al. 2013; Dick et al. 2013). During the past decade, great progress has been made in characterizing the functional organization of the developing infant brain based on the resting-state fMRI (rsfMRI) technique (Biswal et al. 1995; Fransson et al. 2007; Gao et al. 2009b, 2011, 2013; Smyser et al. 2010; Doria et al. 2011; Alcauter et al. 2015). These studies revealed significant, sequential, and patterned growth of different functional networks during infancy with significant behavioral correlations, supporting

the great potential of deriving brain-based biomarkers of risks using rsfMRI-based functional connectivity measures.

However, one difficulty that has been frequently encountered is the lack of infant-specific functional brain parcellations, which are urgently needed for both the definition of infant-specific regions of interests (ROIs) and the interpretation of infant functional connectivity patterns. We have previously propagated the automated anatomical labeling (AAL) brain parcellations from adult to infant space based on structural similarity using a nonlinear registration method (Shi et al. 2011), providing a set of structural brain parcellations for infants. However, there are major limitations in the application of structural brain parcellations in rsfMRI-based functional connectivity studies due to the potential cancellation effects by averaging across heterogeneous BOLD signals within a given ROI (Smith et al. 2011). Recognizing this, different functional brain parcellation schemes have been proposed for adult brain (Bellec et al. 2010; Kim et al. 2010; Lashkari et al. 2010; Mumford et al. 2010; Power et al. 2011; Zhang et al. 2011) but infant-specific functional brain parcellations are yet to be determined.

In this study, we aimed to define a set of normative functional brain parcellations for neonate, 1-, and 2-year olds to facilitate future studies of infant functional development. As the first attempt, we opted to apply the AAL boundary as a spatial constraint given its wide use in functional connectivity studies and the interest to delineate local specialization patterns during infancy within well-defined AAL regions. To achieve this, we modified the original normalized cut (NCUT) approach (Shi and Malik 2000) and incorporated a consistent similarity-based stopping criterion during an iterative process to objectively determine the number of functional subunits within each AAL region across different age groups. Our second aim was to characterize novel functional brain developmental changes in local functional specialization, global functional pattern differentiation, regional connectivity, and whole brain hub distribution based on the newly derived parcellations. Overall, we expect a nonlinear trend featuring more developmental changes during the first year of life (Gao et al. 2009b, 2016). Regionally, we hypothesize increasing levels of local specialization with age within individual AAL regions, especially among primary functional areas. Globally, we expect to see a general "local to distributed" pattern featuring decrease in short-range connections but increase in long-range integrations (Fair et al. 2009; Gao et al. 2011). Particularly, we hypothesize connectivity decrease among bilateral primary sensorimotor regions (Gao et al. 2015) but increase between frontoparietal association regions in the anterior-posterior direction (Gao et al. 2009b, 2015). Finally, regarding hub distribution, we expect to replicate previous findings of a dominance in primary functional areas during infancy (Fransson et al. 2011; Gao et al. 2011) but we also expect novel findings given the difference between the current functional parcellation-based study and previous investigations based on either original AAL region (Gao et al. 2011) or voxel-wise search (Fransson et al. 2011). By deriving a set of normative functional brain parcellations during infancy and delineating the associated novel developmental patterns, we hope our results will facilitate future studies of the normal and abnormal functional brain development (Grewen et al. 2015; Salzwedel et al. 2015, 2016).

Materials and Methods

Subjects and Data Acquisition

An adult data set was first used to test the effectiveness of our functional parcellation methods, which were subsequently applied to our infant data set to derive infant-specific functional parcellations.

Adults

The adult data set was from FCON-1000 project (https://www.nitrc.org/projects/fcon_1000, also see Biswal et al. (2010)). It includes 198 healthy subjects with no brain lesions or mental disorders (Buckner, R.L.; n = 198 [75M]; ages: 18–30 years). Images were acquired at multiple centers using 3T scanners with below parameters: for rsfMRI, $3 \times 3\,mm^3$, TR = 3 s, 119 volumes, and for T1, 1–1.2 mm isotropic resolution.

Infants

The infant data set was part of a large study of early brain development in normal children (Gilmore et al. 2007; Gao et al. 2016); Neonates (n = 230 [106M]; scan age: 272–348 days); 1-year olds (n = 143 [74M]; scan ages: 605–738 days); 2-year olds (n = 107 [64M]; scan ages: 973–1144 days). Inclusion criteria were birth between gestational age of 35 and 42 weeks, appropriate weight for gestational age, and the absence of major pregnancy and delivery complications, as defined in the exclusion criteria. Exclusion criteria included maternal pre-eclampsia, placental abruption, neonatal hypoxia, any neonatal illness requiring greater than 24 h stay at a neonatal intensive care unit, mother with HIV, mother using illegal drugs/narcotics during pregnancy, and any chromosomal or major congenital abnormality. This study was approved by the Institutional Review Board (IRB) of the University of North Carolina at Chapel Hill.

Infant images were acquired using 2 scanners: 1) 3T head-only Siemens Allegra with circular polarization head coil, and 2) 3T Siemens Tim Trio with 32-channel head coil. Functional images were acquired using a T_2^*-weighted EPI sequence: TR = 2 s, TE = 32 ms, 33 slices, and 4 mm isotropic resolution. A total of 150 volumes were acquired in 5 min. Structural images were acquired using a 3D MPRAGE sequence: TR = 1820 ms, TE = 4.38 ms, and 1 mm isotropic resolution.

Preprocessing

Functional data were preprocessed using a common pipeline in the FMRIB (for Functional MRI of the Brain) Software Library (FSL; version 5.0.9) (Jenkinson et al. 2012). Steps included discarding the first 10 volumes (20 s), slice-timing correction, rigid-body motion correction, bandpass filtering (0.01–0.08 Hz), and regression of white matter, CSF, and the 6 motion parameters. Data scrubbing was also implemented; scrubbing criteria, 0.5% signal change and 0.5 mm framewise displacement (Power et al. 2012). Subjects with less than 3 min of functional data after scrubbing were excluded. Structural image skull stripping was doing using FSL and the Analysis of Functional NeuroImages software suite (AFNI version 16.0.19; Cox, 1996). The AFNI script @NoisySkullStrip was used to bolster skull-striping in neonates, which on average demonstrate lower tissue/skull contrast. For each subject and session, after an initial rigid alignment between functional data and T1-weighted, high-resolution structural images, a nonlinear transformation field was obtained from individual T1-weighted images to age-specific T1-template images (Shi et al. 2011). Adult data were aligned to MNI N27 (Holmes et al. 1998; Eickhoff et al. 2007). Finally, the combined transformation field was used to warp the preprocessed rsfMRI data to the template images.

Since the number of voxels can potentially influence the parcellation process, we normalized the total number of brain voxels across age groups, using 2-year old data as a reference.

Specifically, the neonate and 1-year old data were upsampled to 3.751 mm and 2.928 mm isotropic resolution, respectively, resulting in approximately 16 000 total voxels in brain area for each age group.

Method

Proposed Hybrid Iterative Normalized Cut (HI-NCUT) Approach

Flow chart of the proposed iterative NCUT method was provided in Supplementary Figure S1. We formulated the functional parcellation of the brain into a graph-based partitioning problem. Considering the whole brain is composed of tens of thousands of voxels, the goal was to cluster these voxels into structural and functional coherent regions.

Denote $G = (V, W)$ as a weighted graph consisting of a set of vertices $V = \{v_1, v_1, \ldots, v_N\}$ and edges $W = \{w(i, j), v_i, v_j \in V\}$. N is the number of total vertices. $w(i, j)$ is the weight between vertices v_i and v_j, and $w(i, j) = 0$ means they are not connected. In fMRI data scenario, each brain voxel serves as a vertex, and each voxel has a time series. We assigned the weight $w(i, j) = s(v_i, v_j)$ to the edge between voxel v_i and voxel v_j, where the $s(v_i, v_j)$ is their functional connectivity, computed by nonnegative correlation coefficient between their time series. The graph G can be cut into 2 disjoint sets, A and B, with $A \cup B = V$ and $A \cap B = \varnothing$. The cut cost was defined as the sum of the weights on edges connecting voxels in A to voxels in B:

$$\mathrm{cut}(A, B) = \sum_{v_i \in A, v_j \in B} w_{i,j}. \tag{1}$$

Ideally, an optimal graph partition scheme would minimize the cut cost. However, since cutting small sets of isolated nodes in the graph will also satisfy low cut cost, a normalized cost was proposed to avoid this bias. The NCUT was defined as a fraction of the total edge connections to all the nodes in the graph:

$$\mathrm{Ncut}(A, B) = \frac{\mathrm{cut}(A, B)}{\mathrm{assoc}(A, V)} + \frac{\mathrm{cut}(A, B)}{\mathrm{assoc}(B, V)}, \tag{2}$$

where $\mathrm{assoc}(A, V) = \sum_{v_i \in A, v_k \in V} w_{i,k}$ is the sum of weights on edges connecting voxels in A to all the voxels in the graph. Similarly, $\mathrm{assoc}(B, V) = \sum_{v_j \in B, v_k \in V} w_{j,k}$ is the sum of weights on edges connecting voxels in B to all the voxels in the graph. The advantage of NCUT lies in its ability of minimizing the disassociation between the groups, as well as maximizing the association within the groups.

Since NCUT only partitions the graph into 2 parts, one must perform it multiple times to further cut the resulting parts into more small parts to reach the final partition scheme. Previous studies often predefined the final number of clusters, so that NCUT would stop when total cluster reaches that number. In this study, we defined a novel similarity-based stopping criterion to objectively determine the number of functional parcellations. As a data-driven approach, this is especially beneficial when comparing the results from data with multiple age groups, where the change of the whole brain's functional organization could be objectively delineated. Here we defined the stopping criterion as within–between ratio:

$$\mathrm{WB}(A, B) = \frac{\mathrm{within} - \mathrm{between}}{(\mathrm{within} + \mathrm{between})/2}$$

and

where

$$\mathrm{within} = \frac{\mathrm{cut}(A, A) + \mathrm{cut}(B, B)}{N_A(N_A - 1) + N_B(N_B - 1)}, \qquad \mathrm{between} = \frac{\mathrm{cut}(A, B)}{N_A N_B}, \tag{3}$$

where N_A and N_B are the number of voxels in partition A and B.

This within–between ratio was checked each time a NCUT was performed. If it was larger than a given threshold, the partition continued for each of the subparts. The program iterated until the stopping criterion was reached on all partitions. The resulting collection of partitions was considered as the final brain parcellation map.

This method was applied to group correlation matrices based on either the group average (averaging individual correlation matrices) and group aggregate (concatenating times series from individual subjects and calculate one group-representative correlation matrix) approaches and the results were compared.

Structural Constraint Integration

In the last section, we introduced the brain parcellation method based on voxel-wise functional connectivity measures. Recall, we previously developed age-specific structural parcellations for infants (Shi et al. 2011) and here our idea was to incorporate these prior knowledge as structural constraints such that the final parcellation contained structural and functional coherent regions.

Denote a structural graph $H = (V, F)$ to represent the relationship of vertices and edges in our previously proposed structural infant parcellation at a given age. In this case, each brain voxel serves as a vertex and belongs to a structural ROI. The edges F stands for the voxel relationship, where $f(i, j) = 1$ if voxel v_i and voxel v_j belong to the same ROI, and $f(i, j) = 0$ if not. Since the fMRI data have been normalized into the structural space, this graph shares the same voxels V with the previous functional graph. To integrate this structural information into the iterative NCUT in rsfMRI data, we redefined the weight as follows:

$$w_{i,j} = \begin{cases} s(v_i, v_j) & f(i, j) = 1 \\ 0 & f(i, j) = 0 \end{cases}, \tag{4}$$

where the weight is set to 0 if 2 voxels are not in the same structural region. This constrained resulting clusters to follow the structural borders, where voxels in the same structural ROI were parcellated into more functional homogenous regions.

As pointed out by Shen et al., although minimizing NCUT is an NP-complete problem, an approximate discrete solution could solve this problem efficiently (Shen et al. 2010).

Experimental Design

Performance Measures

The lack of ground truth makes it difficult to evaluate the resulting parcellation as well as select parcellation parameters. Here, considering the goal was that the ideal parcellation would have both inter-subject consistency in spatial topology and individual homogeneity in the defined functional units, we evaluated both structural consistency and functional homogeneity within the obtained parcellations.

First, Dice Similarity was used to evaluate the structural consistency between different parcellation results obtained from different subgroups of the original population. The conventional

Dice Similarity compares 2 regions, $DS = 2|A \cap B|/(|A| + |B|)$. Since each parcellation map contains multiple regions and these regions are not necessarily corresponding to the regions in another parcellation map, we defined an Overall Dice Similarity (ODS):

$$\mathrm{ODS} = \frac{\sum_{i \in P_A} \max_{j \in P_B} DS(A_i, B_j) + \sum_{j \in P_B} \max_{i \in P_A} DS(A_i, B_j)}{K_A + K_B}, \quad (5)$$

where K_A and K_B are the total number of partitions in parcellation maps A and B, respectively. Specifically, each region in map A will find a best overlapped region in map B, and similarly each region in map B will find a best overlapped region in map A. The Dice Similarity of all the regions in maps A and B are then averaged into the Overall Dice Similarity. ODS ranges from 0 to 1, with one representing perfect overlap.

Second, we employed the Silhouette Width (SI) to quantify the functional homogeneity within defined parcellations. Given a parcellation map contains K regions, where for the k-th region:

$$SI(k) = \frac{a_k - b_k}{\max\{a_k, b_k\}},$$

where

$$a_k = \frac{1}{n_k(n_k - 1)} \sum_{i,j \in c_k, i \neq j} s(v_i, v_j), \quad (6)$$

$$b_k = \frac{1}{n_k(N - n_k)} \sum_{i \in c_k} \sum_{j \notin c_k} s(v_i, v_j),$$

where c_k is a ROI, n_k is the number of voxels in that ROI, $s(v_i, v_j)$ is the functional connectivity between vertex v_i and v_j. Negative SI values indicate incorrect clustering, and values near 1 represent a superior solution.

Comparisons Across Different Parcellation Methods in Adult Data

To evaluate the consistency of our proposed functional parcellation methods, we randomly separated the 198 adult images into 5 groups with roughly equal numbers. Subsequently, the proposed method was applied on the Group 5 data only to generate a parcellation scheme, referred to as Proposed-Group5 (# of regions = 192, objectively determined by our WB threshold of 50, details on parameter setting in Supplementary Figs S2–S5). The remaining 4 groups served as unseen images to evaluate the representativeness of each parcellation in terms of within-unit functional homogeneity. The proposed parcellation scheme was compared with 3 other brain parcellations: 1) CC et al. (Craddock et al. 2012); a hybrid brain parcellation scheme using rsfMRI functional data and strict local spatial constraints (i.e., each voxel only connects to its 27 nearest neighbors, # of regions = 200); 2) CC-Group5; another parcellation generated by applying CC et al.'s clustering method to our Group 5 data (# of regions = 200), using the pyClusterROI software (http://ccraddock.github.io/cluster_roi/); and 3) YJ et al. (Jin et al. 2015); a structural-based parcellation by subdividing the original AAL template into subregions with similar sizes using seeds from cubic parcellation and region growing (# of regions = 203).

Control Analyses for Functional Parcellation of the Infant Brain

A series of testing/control analyses were carried out to better stratify the resulting infant-specific functional parcellations. First, similar as in adult, we evaluated the consistency of group-level parcellations by separating the infant data at each age into 2 groups. One group was used to generate the parcellation scheme and the other group was used for evaluation of the functional homogeneity. The proposed method and 3 other comparison parcellations were all evaluated, including 1) CC et al.; obtained by aligning their original parcellation to each of the infant groups using nonlinear registration method ANTS (Avants et al. 2011), 2) CC-Group2; generated by applying CC et al.'s clustering method to the Group 2 data with the pyClusterROI software within their mask, and 3) YJ et al.; generated by applying their anatomical parcellation method on the age-specific AAL templates. Second, since the infant data were acquired from 2 MR scanners, we limited our data to those acquired using the same scanner to rule out the effect of 2 scanners on the resulting parcellation. Third, the subjects had different number of time points after the data scrubbing approach in image preprocessing. To evaluate that effect, we matched the number of remaining number of rsfMRI volumes across the 3 age groups and compared the resulting parcellation to test the potential effects of differential motion contamination. Finally, we assessed parcellations derived directly from individual subjects to demonstrate the individual variability in functional parcellation.

Characterization of Developmental Changes

The newly defined parcellations could serve as age-specific templates for cross-sectional functional connectivity investigations. Moreover, they could be used to delineate longitudinal changes in functional connectivity if such data are available. In this study, we sought to characterize several domains of novel longitudinal changes based on our newly derived parcellation schemes. First, 3 representative areas (including both primary areas of bilateral pre/postcentral gyrus and higher-order areas of the insula) were selected to demonstrate the developmental changes of local subdivisions across age groups. Second, a functional specialization index (FSI) was derived to quantify the changes in local functional specialization as indicated by the associated global functional connectivity patterns. Specially, the 2-year final subunit division map within each AAL area was used as a template and warped back to neonates and 1-year olds to calculate the mean cross-correlations of their whole brain functional connectivity patterns. Subsequently, 1 minus the mean correlation was calculated as the FSI which ranged from 0 to 1, with higher value indicating higher levels of functional specializations across different functional subunits. Then, we performed statistical analysis on the FSI values to detect significant increases or decreases for all AAL regions. Third, longitudinal changes (i.e., increase/decrease) of pair-wise functional connectivity changes were detected and their associated topological features were characterized. Specifically, a linear mixed effect (LME) model was applied to each pair-wise connection to measure its change associated with age. The fixed-effect model is: $FCz \sim 1 + \log \mathrm{Age} + \mathrm{Gender} + \mathrm{BirthWeight} + FD + \mathrm{Scanner} + \mathrm{GAge}$, where FCz is the functional correlation strength, FD is residual framewise displacement, Scanner is the index of scanner used, and GAge is gestational age at birth. Random effects for intercept and log Age term were also added. A stringent threshold of $P < 0.001$ after FDR correction was defined to feature the most robust developmental changes in regional connectivity (results with $P < 0.05$ after FDR correction were included in Supplementary Material). Finally, we characterized the developmental changes in whole brain functional topography in

terms of hub distributions based on betweeness-centrality measures through graph-theoretical analyses (Rubinov and Sporns 2010). Specifically, the parcellations were used as nodes and functional connectivity from the data were used as edges to form the brain network. Betweeness-centrality was defined as the fraction of the shortest paths between any pairs of nodes that travel through the node, and the nodes with value larger than the mean plus standard deviation were classified as the hub nodes. The derived distributions were also compared across different brain parcellation schemes.

Experimental Results

Adult Data

Figure 1A shows the 2D and 3D views of the proposed parcellation (based on WB = 50, details on parameter setting in Supplementary Figs S2–S5) together with 3 comparison schemes. Qualitatively, the proposed solution was distinct in appearance featuring irregular ROI shapes and sizes compared with other schemes (i.e., more sphere-like in shape with similar sizes). Indeed, ROI size in the proposed parcellation showed a much greater range (Fig. 1B) compared with the other parcellations. The effectiveness of all 4 parcellation schemes were compared by evaluating the functional homogeneity (SI) of each defined functional subunit based on the 4 testing data sets (Groups 1–4). Figure 1C demonstrates that the proposed parcellation scheme achieved the highest SI values, effectively outperforming other comparison parcellations in each subset ($P < 0.001$ for all 3 comparisons between the proposed scheme and other schemes). Overall, a 2-way ANOVA with SI as the observation, and group and method as the 2 factors confirmed that the sum of square differences across testing groups (1–4)

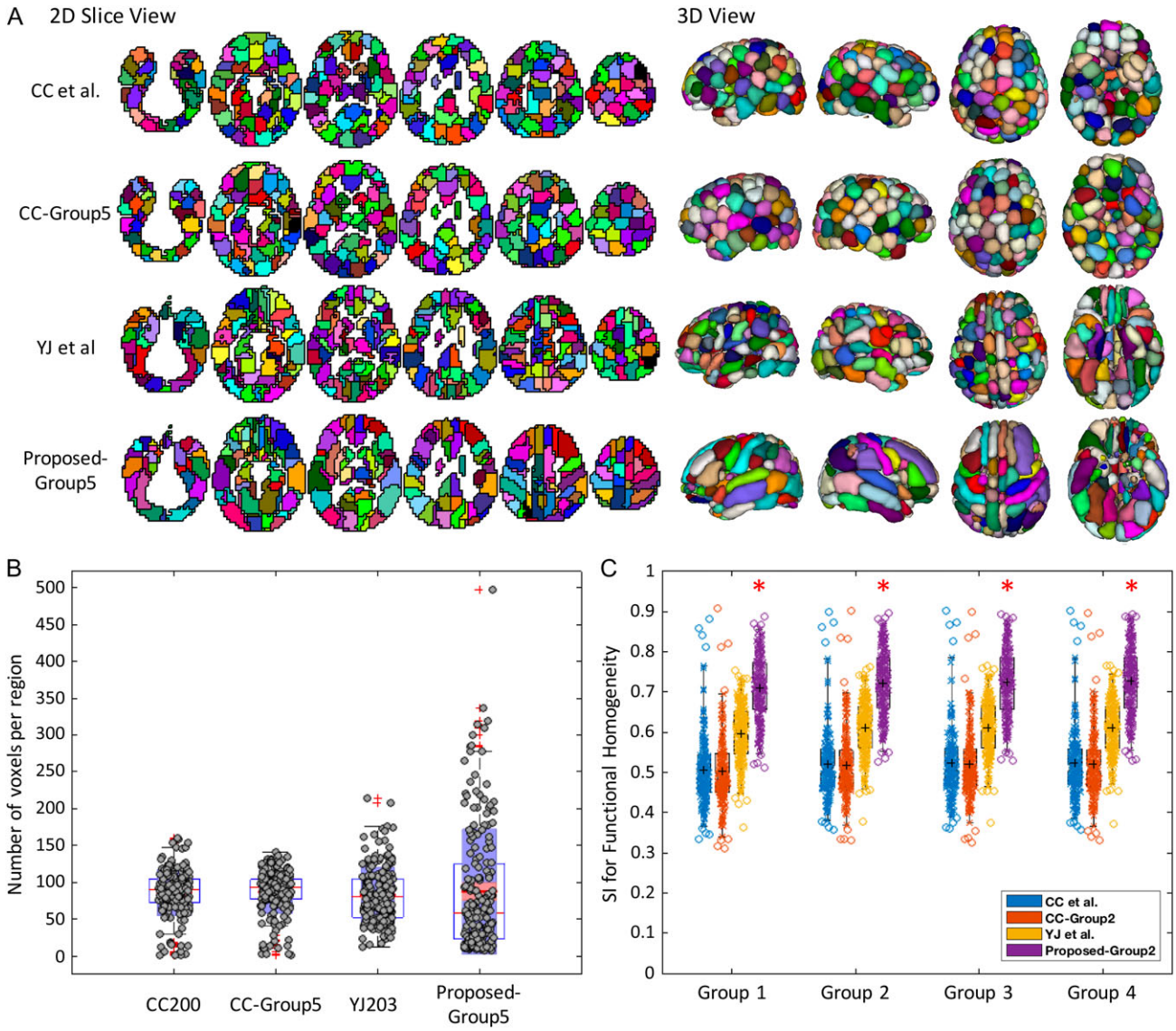

Figure 1. Illustration of the brain parcellation maps in the proposed and comparison parcellations. (A) Shows 6 axial 2D slices, and 3D rendering results with the right, left, top, and bottom views are provided. Note that random colors were used for visualizing different regions. (B) Shows the boxplot of the number of voxels in the ROIs for different parcellations, and (C) Shows the boxplot of SI values for different brain parcellations in subject Groups 1–4. The circles in boxplots represent parcellated functional regions. Denoted by *, the proposed scheme demonstrates statistically higher SI when compared with each of the 3 other schemes ($P = 8.2e{-}74/4.2e{-}75/2.3e{-}38$, respectively).

was small (i.e., 0.00075, $P = 1.4e{-}11$) but across methods was drastic (i.e., 0.11, $P = 2.2e{-}21$).

Infant Data

Next, we applied the proposed iterative NCUT algorithm (WB = 50) on the Group 2 data of neonate, 1 year, and 2 years. Figure 2A shows the 2D and 3D views of the resulting parcellations, and Figure 2B shows the 3D views of the comparison parcellations. In the Group 1 evaluation data (Fig. 2C), our analyses showed high levels of within-unit homogeneity (SI: mean 0.82/0.79/0.78 for 0, 1, and 2-year olds) for parcellations derived from each subunit, which were significantly higher than all 3 other comparison schemes ($P < 0.001$). The Group 2 solution also demonstrated high levels of similarity with the whole-group representations (ODS: mean 0.89/0.87/0.83 for 0, 1, and 2-year olds).

Control Analysis

First, given that the number of subjects was heavily biased for scanner-1 (Trio; 186 out of 230 in neonates (81%), 124 out of 143 in 1 year (87%), and 93 out of 107 in 2 years (87%)), we repeated our analysis based on scanner-1 data alone. Our results showed slightly higher levels of SI (0.84/0.80/0.80 for 0/1/2-year olds, compared with 0.83/0.80/0.80 for 0/1/2-year olds) but 2 sample t-tests confirmed that such differences did not reach statistical significance (P values of 0.65, 0.73, 0.97 for 0/1/2-year olds). Moreover, the structural consistency between the scanner-1 solution and the whole-group solution was also high (ODS = 0.89/0.90/0.87 for 0/1/2-year olds). Second, given that the number of remaining rsfMRI volumes after preprocessing was significantly lower in neonates (130) than that of 1-year and 2-year olds (137 for both groups), we removed neonatal subjects with the lowest number of remaining rsfMRI volumes untill the mean time points equalled 137 to match that in 1 and 2-year olds. The resulting neonatal parcellation was highly consistent with our primary results (ODS 0.88) and the mean SI also did not change (mean SI 0.83), suggesting robustness of our results against slight differences in number of volumes post-scrubbing. Finally, to evaluate the variability of parcellations from individual subjects, we randomly selected 20 subjects for each age group. Results show much lower function homogeneity (SI: 0.57/0.55/0.53 for 0/1/2-year olds) and anatomical overlapping with the whole-group parcellations (ODS: 0.42/0.41/0.37 for 0/1/2-year olds). This indicates the variability is relative large between individual subjects while the group average is more stable and preferred strategy to extract population patterns.

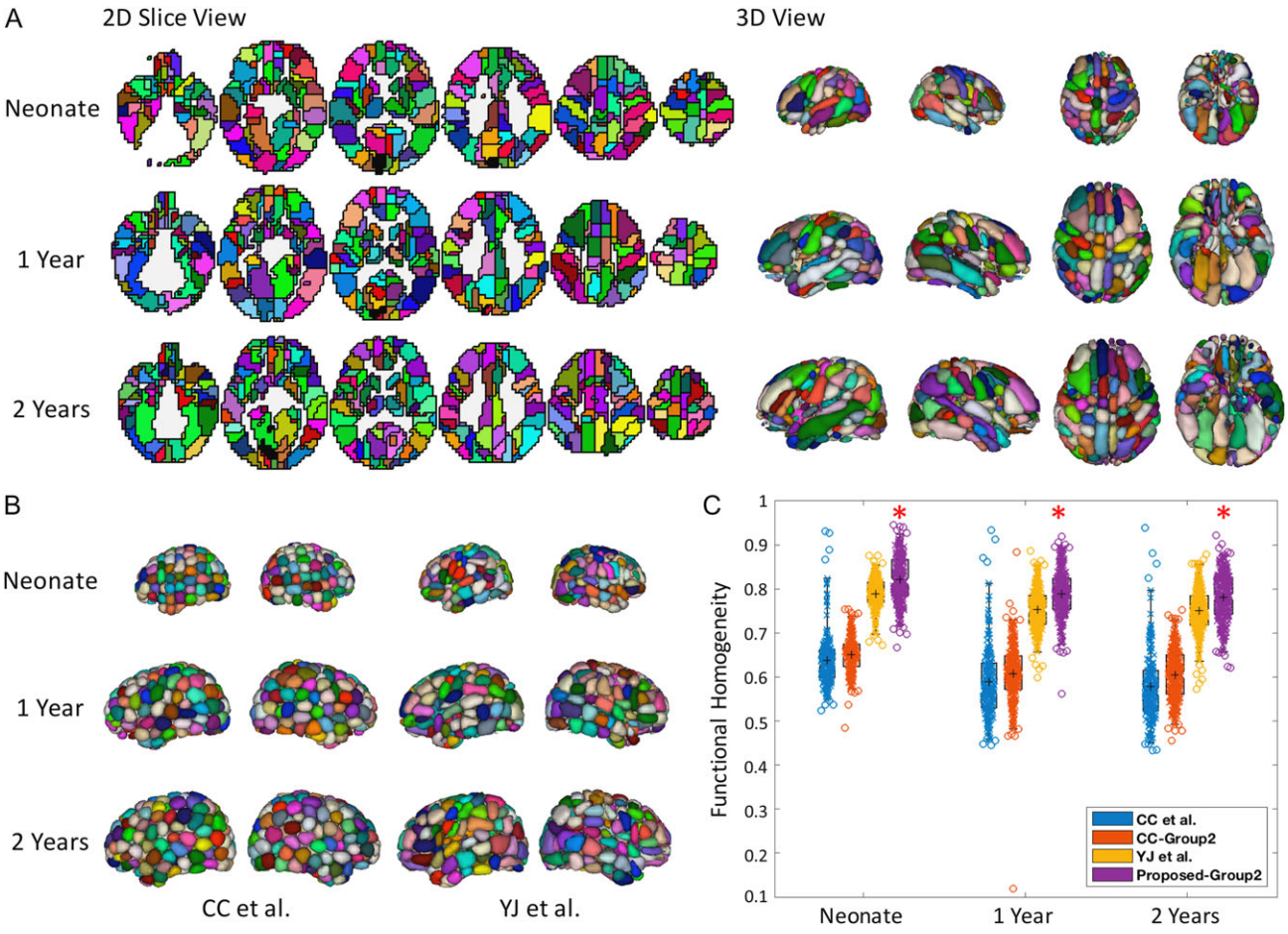

Figure 2. Illustration of the brain parcellation maps in neonates, 1-year olds, and 2-year olds. (*A*) Shows 6 axial 2D slices, and 3D rendering results, where the right, left, top, and bottom views are provided for the parcellations based on infant Group 2 data. Note that since the parcellations of 3 age groups have different sizes, roughly similar 2D slices are selected to be shown and the size difference could be observed in 3D view. (*B*) Shows the 3D views of 2 comparison methods, and (*C*) is the boxplot of functional homogeneity, evaluated on the Group 1 infant data. The circles in boxplots represent parcellated functional regions. Denoted by *, the proposed scheme demonstrates statistically higher SI when compared with each of the 3 other schemes ($P = 8.3e{-}113/8.5e{-}129/5.1e{-}11$, respectively).

Developmental Changes

Overall, the total number of functional subunits increased as a function of age: 223 in neonates, 258 in 1-year olds, and 278 in 2-year olds, supporting our hypothesis of a general trend of increasing levels of local specialization. The ODS between neonates' functional parcellation and 1-year olds' was lower (0.51) than that between 1 and 2-year olds (0.56) suggesting more developmental changes in local subdivision during the first year of life. Indeed, the FSI, quantifying the level of local specialization based on the associated global functional connectivity patterns, progressively increased at whole brain level (mean: 0.47/0.56/0.60 for 0/1/2-year olds). Regionally, 60 out of 76 AAL regions (i.e., those showing local subdivisions after the proposed functional clustering in 2-year olds) demonstrated significantly enhanced differentiation with respect to global functional connectivity patterns (i.e., FSI) when comparing neonates with 1-year old (3 showing no changes while 13 regions showing decrease). When comparing 1-year with 2-year olds, 46 out of 76 regions showed enhanced differentiation (5 regions showing no significant changes and 25 showing decrease), again supporting the nonlinear development of local specialization featuring more changes during the first year (see Supplementary Fig. S6 for all regions).

Examples of age-dependent changes in local subdivisions are presented in Figure 3A. As hypothesized, the bilateral pre- and postcentral gyrus became more differentiated along the medial-lateral axis, which is highly consistent with the sensorimotor homunculus layout (number of subunits in left/right precentral gyrus: 2/3, 3/4, 8/5; in left/right postcentral gyrus: 1/1, 3/3, 3/3; for neonates, 1-year, and 2-year olds, respectively). Intriguingly, the left precentral gyrus demonstrated considerably more fine separations than the right during the second year of life (i.e., from 3 to 8 for left precentral versus from 4 to 5 for the right precentral gyrus). In contrast, the higher-order functional area of the insula maintained consistent anterior-posterior segregation that is highly in line with adult findings and our previous reports on infants (Alcauter et al. 2015). All precentral and postcentral regions demonstrated significantly enhanced FSI with age (Fig. 3B), which is highly consistent with the increasingly differential global functional connectivity patterns with age for all subdivisions (Fig. 3C). Interestingly, asymmetry is found in insula where increasing FSI is observed in the left side over time but not in the right side, suggesting that the functional specialization of right insula reaches a similar level in neonates compared with 1 year and 2 years of age (Biduła and Króliczak 2015).

When assessing whole brain functional connectivity changes, the expected local to distributed pattern was evident (Fig. 4A) and the anatomical distances associated with increasing connections were significantly longer than those associated with decreasing connections (Fig. 4B). Moreover, increasing connections largely focused on bilateral occipital connections (28%), frontal-parietal connections (20%), parietal-temporal connections (13%), and subcortical-cortical connections (17% for combined subcortical-occipital/parietal/frontal connections, Fig. 4C). In contrast, age-related decreases concentrated on within-lobe connections (i.e., within subcortical 25%, within central 14%, within temporal 7%). Finally, when evaluating whole brain hub distribution using betweenness centrality measures, interesting developmental patterns were also observed (Fig. 4D): 1) consistent with our expectation, all 3 infant groups possessed hubs in primary sensorimotor (e.g., PreCG. L, PCL. R, SMA. L in neonates; PreCG. L, PCL. R, in 1-year olds; and PreCG. L/R, PoCG. L/R, SMA. R in 2-year olds), visual (e.g., MOG. R, CAL. L in neonates; IOG. R in 1-year olds; and MOG. R in 2-year olds), and auditory cortices (e.g., MTG. R in neonates; MTG. R in 1-year olds; and MTG. L/R in 2-year olds); and 2) a novel

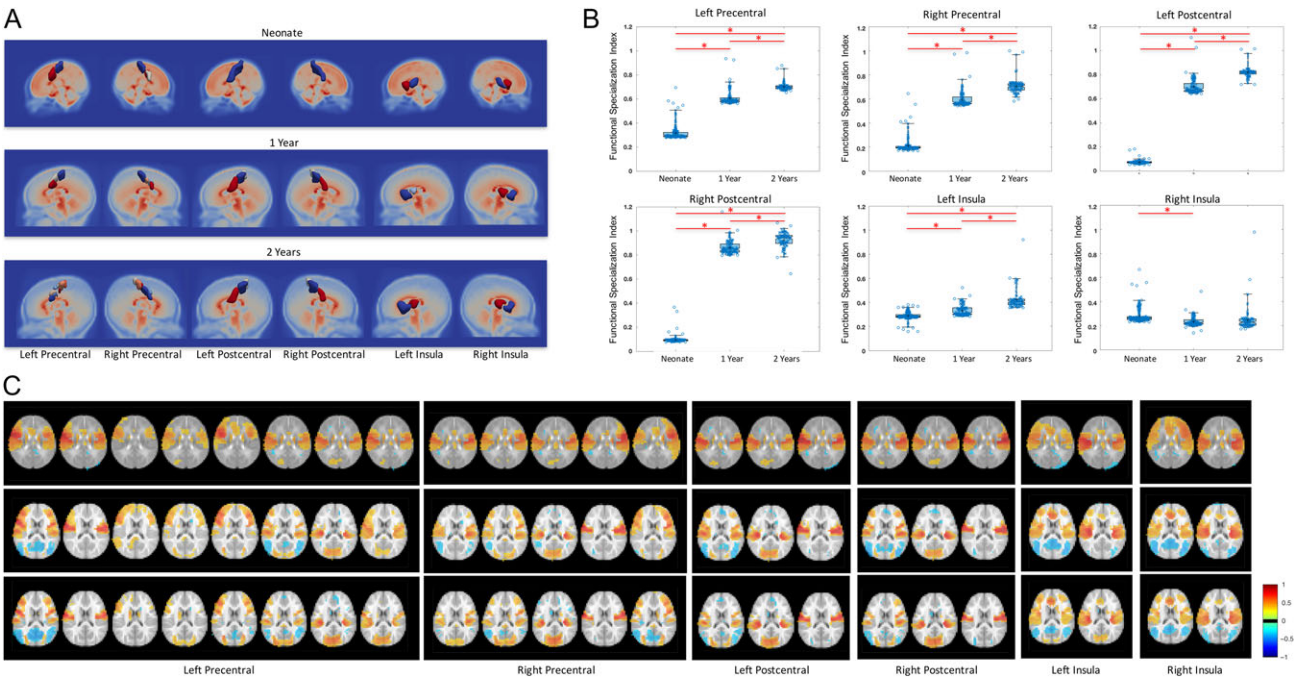

Figure 3. Demonstration of age-dependent subunit changes. (A) Subunit topologies in 5 representative areas in the 3 infant groups. (B) Boxplot of the mean correlations of whole brain connectivity map between each pair of subunits in the representative areas. The circles in boxplots represent FSI in individual subjects; *'s indicate significant differences ($P < 0.001$) between 2 age groups. (C) Illustration of the whole brain connectivity maps using the subunits in 2 years as seed regions. In each panel, from left to right are for different subunits, and from top to bottom are for neonate, 1 year, and 2 years.

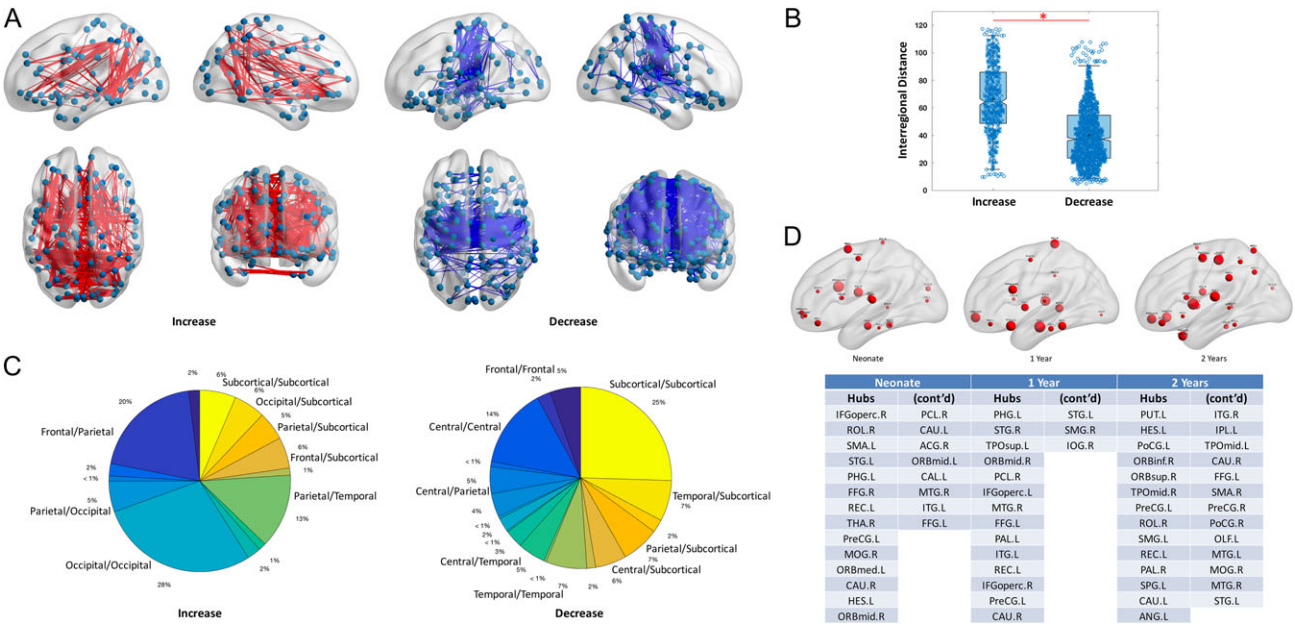

Neonate		1 Year		2 Years	
Hubs	(cont'd)	Hubs	(cont'd)	Hubs	(cont'd)
IFGoperc.R	PCL.R	PHG.L	STG.L	PUT.L	ITG.R
ROL.R	CAU.L	STG.R	SMG.R	HES.L	IPL.L
SMA.L	ACG.R	TPOsup.L	IOG.R	PoCG.L	TPOmid.L
STG.L	ORBmid.L	ORBmid.R		ORBinf.R	CAU.R
PHG.L	CAL.L	PCL.R		ORBsup.R	FFG.L
FFG.R	MTG.R	IFGoperc.L		TPOmid.R	SMA.R
REC.L	ITG.L	MTG.R		PreCG.L	PreCG.R
THA.R	FFG.L	FFG.L		ROL.R	PoCG.R
PreCG.L		PAL.L		SMG.L	OLF.L
MOG.R		ITG.L		REC.L	MTG.L
ORBmed.L		REC.L		PAL.R	MOG.R
CAU.R		IFGoperc.R		SPG.L	MTG.R
HES.L		PreCG.L		CAU.L	STG.L
ORBmid.R		CAU.R		ANG.L	

Figure 4. Demonstration of developmental changes. (*A*) Increased (left panel) and decreased (right panel) functional connections with age in LME model. Most robust changes are highlighted here with $P < 0.001$ FDR corrected (see Supplementary Fig. S8 for $P < 0.05$ with FDR corrected). (*B*) Boxplot of the interregional distance (mm) for the increased and decreased connections. The circles in boxplot represent different connections; *indicates the increased connections have significant longer distance than that of decreased connections ($P < 0.001$). (*C*) Pie plot shows the percentage of changes between major brain lobes where the regions are labeled when no less than 5%. (*D*) Hub distributions for all age groups from the parcellations of the proposed method and a ranked list of hubs in all age groups. The node size reflects the relative strength of betweenness centrality.

pattern of orbital frontal areas as hubs was consistently observed for all 3 age groups (e.g., ORBmid. L, ORBmid. R, ORBmed. L in neonates; ORBmid. R in 1-year olds; and ORBsup. L, ORBinf. R in 2-year olds).

Discussion

In this paper, we derived a set of normative functional brain parcellations for infants aged between 3 weeks and 2 years of age. Through functional connectivity-based clustering with AAL boundary constraint, our parcellations ensured the definition of local subunits with homogenous functional representations. Indeed, our results in both adults and infants showed higher levels of within-unit functional homogeneity than that of other comparison parcellations. Developmentally, nonlinear, local to distributed functional connectivity developmental trends were revealed using the newly derived functional parcellations featuring both expected and novel findings.

Brain parcellations are widely used in functional connectivity-based studies of the brain's functional mechanisms. Two major applications include: 1) the definition of seed regions for seed-based functional connectivity analyses; and 2) the application of the entire parcellation to segment the whole brain into a predefined number of regions for graph theory-based analyses. In both cases, the underlying assumption is functional homogeneity within each ROI. However, this assumption is rarely fulfilled when using structurally defined brain parcellations. In fact, Smith et al. have elegantly conducted simulations demonstrating that even with a moderate mixing of time series (20%) from different ROIs, the resulting sensitivity of detecting correlations with the target ROI drop from 90% to 20% for many correlation estimation methods (Smith et al. 2011). Empirically, Wang et al. also showed significant differences in multiple brain functional connectome properties when using different structural parcellations on fMRI images, underscoring the effects of parcellation selection on resulting functional brain investigations (Anand et al. 2009). In light of this, different functional parcellations are derived for adults. However, functional-based brain parcellations specifically designed for infants are lacking. The dramatic functional development process prohibits direct translation of adult functional parcellations to infants thus the currently derived infant-specific parcellations could be of high importance for future studies of early functional brain development. To the best of our knowledge, this is the first set of normative functional brain parcellations derived specifically for infant populations. The proposed parcellations could serve as a common coordinate space and thus better facilitate comparisons across studies.

There are 3 major advantages of the currently derived infant-specific functional brain parcellations. The first one is the higher level of functional homogeneity compared with other established functional brain parcellations as shown in Figure 2. Carddock et al. defined a strict structural constraint (i.e., each voxel only connects with its 26 nearest neighbors) (Craddock et al. 2012), which likely explains the similarly sized sphere-like ROIs in their parcellations (Fig. 2) with relatively lower functional homogeneity. Indeed, Craddock et al. have shown that their approach yields similar results after introducing random functional relationships (i.e., discarding the inherent correlation relationships). The proposed approach, although constrained by AAL boundaries, defines sub-regions purely based on their functional similarity, resulting in higher in-unit functional homogeneity compared with CC et al./YJ et al. This represents important improvements since, again, a small mix of signals can have devastating effects on the resulting correlation estimation (Smith et al. 2011). Given the wide usage of AAL, one added benefit of following AAL boundaries is that each

resulting functional unit can be readily linked with an anatomical annotation from the AAL parcellation. Second, we incorporated a novel similarity-based stopping criterion to objectively define the number of regions, which can be consistently applied across different age groups. Therefore, developmental changes in the number of local functional specialization can be studied in a more objective way. Finally, our large sample sizes (N = 230, 143, and 107 for neonates, 1 year, and 2-year olds, respectively) allowed us to do reproducibility analyses, effectively demonstrating high levels of functional subunit definition consistency across different subsamples for the proposed method (>80%). Such robustness is critical for the resulting functional brain parcellations to be representative and applicable for independent studies. In the future, the generalizability of our parcellations to infants associated with different risk factors (e.g., prenatal drug exposures) (Grewen et al. 2015; Salzwedel et al. 2015, 2016) will be tested.

Developmentally, there is an increasing trend for the total number of brain parcellations from neonate to 2 years (i.e., 223 in neonates, 258 in 1-year olds, and 278 in 2-year olds for WB = 50; other WB thresholds produce similar trends too, see Supplementary Fig. S5), confirming our hypothesis of increasing levels of local specialization. This is especially true among primary areas as shown in Supplementary Figure S7; areas showing increasing numbers of subunits concentrate more on precentral and postcentral gyrus from neonates to 1-year olds but shift to frontal and temporal regions from 1-year to 2-year olds. This pattern of local specialization from primary to higher-order areas is highly consistent with our previous delineation of the sequential maturation of associated functional networks (Gao et al. 2015), suggesting potential parallel development of local specialization and global integration. More specifically, the left precentral gyrus develops considerably more fine subdivisions during the second year than the right (Fig. 3A). This may indicate lateralized development reflecting better fine motor functions of the right hand, which is consistent with the early emergence of handedness, given the predominance (~90%) of right-handedness in the general population (Scharoun and Bryden 2014). For the insula, we replicated our previous finding of functional segregation along the anteroposterior direction in all 3 age groups starting from neonates (Alcauter et al. 2015). However, when we quantified developmental changes in local specialization based on global connectivity patterns, the left insula demonstrated age-dependent increase in specialization while the right failed, again implying certain level of left-right asymmetry in development. The reported findings that the left insula relates more to parasympathetic effects while the right insula is more involved in sympathetic effects (Caspi et al. 2005; Chiarello et al. 2013) may underlie such asymmetry. Detailed interpretations of each AAL region's fine subdivisions is beyond the scope of this paper and deserves further study.

When examining global functional connectivity changes, our results confirmed the local to distributed trend (Fig. 4B) during early brain development (Gao et al. 2011). Importantly, although the increasing long-range connections cover all 3 major directions of white matter fibers, including commissural (especially within the occipital lobe), association (especially frontal-parietal and parietal-temporal), and projection (subcortical-cortical) directions, as in line with our previously reported major white matter tracts development trend during this period (Gao et al. 2009a), the large contribution of frontoparietal connections (i.e., 20%, second highest next to bilateral occipital connections of 28%) is consistent with our previous delineation of the fast synchronization of the default-mode network during this period (Gao et al. 2009b, 2013). In contrast to long-distance integrations, local specialization occurs more within lobes and almost never occur in association direction (e.g., frontal-parietal and parietal-temporal), suggesting drastic differences in the topological distribution between integration and specialization. Specifically, as expected, decrease in connectivity focus particularly on primary sensorimotor and subcortical areas, which is in line with our previous reports of sensorimotor network specialization (Gao et al. 2015) and thalamic functional differentiation during early brain development (Alcauter et al. 2014). Finally, the distribution patterns of whole brain connection hugs based on the newly derived functional parcellations confirmed major contributions from primary functional regions (Fransson et al. 2011; Gao et al. 2011) but also revealed a novel pattern of orbital frontal hubs during infancy, likely reflecting the important role of attachment during early brain and behavioral development (Minagawa-Kawai et al. 2009).

Several limitations deserve further discussion. The first one relates to thresholding; although we designed a novel data-driven stopping criterion which enabled the selection of a finite number of total areas in an objective and consistent fashion across different age groups our results are still dependent on the selection of the WB threshold. We chose to present a WB threshold of 50 yielding around 200 regions in adult data for fair comparison with other methods (Supplementary Fig. S2). Moreover, our simulations also suggest it is a balance point for the reproducibility between functional homogeneity and structural consistency (Supplementary Fig. S4). However, we recognize that it is still an open question as to what is an optimal representation of the brain's functional organization. Therefore, we provide different sets of parcellations at different thresholds such as WB of 30, 40, 50, and 60 (results are shown in Supplementary Fig. S5), and will make them available to the public via the NITRC repository (https://www.nitrc.org/projects/functionalatlas). Another limitation relates to the application of AAL boundaries as the spatial constraint. This constraint was chosen mainly because of 2 considerations: 1) the wide application of AAL in functional connectivity studies in both adult and infant studies, and 2) the added spatial constraint reduces computational complexity and helped maintain the local contiguity of the resulting functional parcellations. However, future efforts without this spatial constraint, or possibly using different spatial constraints, are needed to compare and/or expand the current parcellations. We also note that there is a recently developed multi-modal adult brain parcellation (Glasser et al. 2016) but priors obtained from this adult parcellation could not be directly translated to infant parcellation construction given the known dramatic developmental changes. However, future explorations using similar gradient-based parcellation approaches are deserved to compare with the current parcellations. Nevertheless, given the goal of deriving the most functionally homogenous ROIs to facilitate rsfMRI studies of the developing brain, the benefits of incorporating multi-modal MRI data sets to this specific aim remains to be determined. Finally, the potential of deriving and applying individual-specific functional parcellations deserves further investigation.

In conclusion, based on a novel iterative NCUT method combining a spatial constraint and a data-driven stopping criterion, we derived the first set of normative functional brain parcellations for infants aged between 3 weeks and 2 years of age. Novel developmental patterns associated with this set of functional parcellations were also delineated. With improved in-unit functional homogeneity and high levels of specificity to infant data we hope the derived functional parcellations will

facilitate future functional characterization of the developing brain.

Supplementary Material

Supplementary material is available at *Cerebral Cortex* online.

Funding

This study was supported by NIH grants (R01MH064065, R01HD05300 to J.H.G.; R21NS088975, R03DA036645-01 to W.G.) and Cedars-Sinai Institutional Support to W.G.

Notes

Conflict of Interest: The authors declare no competing financial interests.

References

Alcauter S, Lin W, Smith JK, Gilmore JH, Gao W. 2015. Consistent anterior–posterior segregation of the insula during the first 2 years of life. Cereb Cortex. 25:1176–1187.

Alcauter S, Lin W, Smith JK, Short SJ, Goldman BD, Reznick JS, Gilmore JH, Gao W. 2014. Development of thalamocortical connectivity during infancy and its cognitive correlations. J Neurosci. 34:9067–9075.

Anand A, Li Y, Wang Y, Lowe MJ, Dzemidzic M. 2009. Resting state corticolimbic connectivity abnormalities in unmedicated bipolar disorder and unipolar depression. Psychiatry Res. 171:189–198.

Avants BB, Tustison NJ, Song G, Cook PA, Klein A, Gee JC. 2011. A reproducible evaluation of ANTs similarity metric performance in brain image registration. Neuroimage. 54: 2033–2044.

Bellec P, Rosa-Neto P, Lyttelton OC, Benali H, Evans AC. 2010. Multi-level bootstrap analysis of stable clusters in resting-state fMRI. Neuroimage. 51:1126–1139.

Biduła SP, Króliczak G. 2015. Structural asymmetry of the insula is linked to the lateralization of gesture and language. Eur J Neurosci. 41:1438–1447.

Biswal B, Yetkin FZ, Haughton VM, Hyde JS. 1995. Functional connectivity in the motor cortex of resting human brain using echo-planar MRI. Magn Reson Med. 34:537–541.

Biswal BB, Mennes M, Zuo XN, Gohel S, Kelly C, Smith SM, Beckmann CF, Adelstein JS, Buckner RL, Colcombe S, et al. 2010. Toward discovery science of human brain function. Proc Natl Acad Sci USA. 107:4734–4739.

Braakman HM, Vaessen MJ, Jansen JF, Debeij-van Hall MH, de Louw A, Hofman PA, Vles JS, Aldenkamp AP, Backes WH. 2013. Frontal lobe connectivity and cognitive impairment in pediatric frontal lobe epilepsy. Epilepsia. 54:446–454.

Burton H, Dixit S, Litkowski P, Wingert JR. 2009. Functional connectivity for somatosensory and motor cortex in spastic diplegia. Somatosens Mot Res. 26:90–104.

Camfield CS, Camfield PR, Gordon K, Wirrell E, Dooley JM. 1996. Incidence of epilepsy in childhood and adolescence: a population-based study in Nova Scotia from 1977 to 1985. Epilepsia. 37:19–23.

Caspi A, Moffitt TE, Cannon M, McClay J, Murray R, Harrington H, Taylor A, Arseneault L, Williams B, Braithwaite A, et al. 2005. Moderation of the effect of adolescent-onset cannabis use on adult psychosis by a functional polymorphism in the catechol-O-methyltransferase gene: longitudinal evidence of a gene X environment interaction. Biol Psychiatry. 57: 1117–1127.

Chiarello C, Vazquez D, Felton A, Leonard CM. 2013. Structural asymmetry of anterior insula: behavioral correlates and individual differences. Brain Lang. 126:109–122.

Craddock RC, James GA, Holtzheimer PE 3rd, Hu XP, Mayberg HS. 2012. A whole brain fMRI atlas generated via spatially constrained spectral clustering. Hum Brain Mapp. 33:1914–1928.

Dick AS, Raja Beharelle A, Solodkin A, Small SL. 2013. Interhemispheric functional connectivity following prenatal or perinatal brain injury predicts receptive language outcome. J Neurosci. 33:5612–5625.

Doria V, Beckmann CF, Arichi T, Merchant N, Groppo M, Turkheimer FE, Counsell SJ, Murgasova M, Aljabar P, Nunes RG, et al. 2011. Emergence of resting state networks in the preterm human brain. Proc Natl Acad Sci USA. 107:20015–20020.

Eickhoff SB, Paus T, Caspers S, Grosbras MH, Evans AC, Zilles K, Amunts K. 2007. Assignment of functional activations to probabilistic cytoarchitectonic areas revisited. Neuroimage. 36:511–521.

Fair DA, Cohen AL, Power JD, Dosenbach NU, Church JA, Miezin FM, Schlaggar BL, Petersen SE. 2009. Functional brain networks develop from a "local to distributed" organization. PLoS Comput Biol. 5:e1000381.

Fransson P, Aden U, Blennow M, Lagercrantz H. 2011. The functional architecture of the infant brain as revealed by resting-state fMRI. Cereb Cortex. 21:145–154.

Fransson P, Skiold B, Horsch S, Nordell A, Blennow M, Lagercrantz H, Aden U. 2007. Resting-state networks in the infant brain. Proc Natl Acad Sci USA. 104:15531–15536.

Gao W, Alcauter S, Elton A, Hernandez-Castillo CR, Smith JK, Ramirez J, Lin W. 2015. Functional network development during the first year: relative sequence and socioeconomic correlations. Cereb Cortex. 25:2919–2928.

Gao W, Gilmore JH, Giovanello KS, Smith JK, Shen D, Zhu H, Lin W. 2011. Temporal and spatial evolution of brain network topology during the first two years of life. PLoS One. 6: e25278.

Gao W, Gilmore JH, Shen D, Smith JK, Zhu H, Lin W. 2013. The synchronization within and interaction between the default and dorsal attention networks in early infancy. Cereb Cortex. 23:594–603.

Gao W, Lin W, Chen Y, Gerig G, Smith JK, Jewells V, Gilmore JH. 2009. Temporal and spatial development of axonal maturation and myelination of white matter in the developing brain. Am J Neuroradiol. 30:290–296.

Gao W, Lin W, Grewen K, Gilmore JH. 2016. Functional connectivity of the infant human brain: plastic and modifiable. Neuroscientist. doi: 10.1177/1073858416635986.

Gao W, Zhu H, Giovanello KS, Smith JK, Shen D, Gilmore JH, Lin W. 2009. Evidence on the emergence of the brain's default network from 2-week-old to 2-year-old healthy pediatric subjects. Proc Natl Acad Sci USA. 106:6790–6795.

Gilmore JH, Lin W, Prastawa MW, Looney CB, Vetsa YS, Knickmeyer RC, Evans DD, Smith JK, Hamer RM, Lieberman JA, et al. 2007. Regional gray matter growth, sexual dimorphism, and cerebral asymmetry in the neonatal brain. J Neurosci. 27:1255–1260.

Gilmore JH, Shi F, Woolson SL, Knickmeyer RC, Short SJ, Lin W, Zhu H, Hamer RM, Styner M, Shen D. 2012. Longitudinal development of cortical and subcortical gray matter from birth to 2 years. Cereb Cortex. 22:2478–2485.

Glasser MF, Coalson TS, Robinson EC, Hacker CD, Harwell J, Yacoub E, Ugurbil K, Andersson J, Beckmann CF, Jenkinson M, et al. 2016. A multi-modal parcellation of human cerebral cortex. Nature. 536:171–178.

Grewen K, Salzwedel AP, Gao W. 2015. Functional connectivity disruption in neonates with prenatal marijuana exposure. Front Hum Neurosci. 9:601.

Holmes CJ, Hoge R, Collins L, Woods R, Toga AW, Evans AC. 1998. Enhancement of MR images using registration for signal averaging. J Comput Assist Tomogr. 22:324–333.

Jenkinson M, Beckmann CF, Behrens TE, Woolrich MW, Smith SM. 2012. FSL. Neuroimage. 62:782–790.

Jin Y, Wee CY, Shi F, Thung KH, Ni D, Yap PT, Shen D. 2015. Identification of infants at high-risk for autism spectrum disorder using multiparameter multiscale white matter connectivity networks. Hum Brain Mapp. 36: 4880–4896.

Karevold E, Roysamb E, Ystrom E, Mathiesen KS. 2009. Predictors and pathways from infancy to symptoms of anxiety and depression in early adolescence. Dev Psychol. 45: 1051–1060.

Kim JH, Lee JM, Jo HJ, Kim SH, Lee JH, Kim ST, Seo SW, Cox RW, Na DL, Kim SI, et al. 2010. Defining functional SMA and pre-SMA subregions in human MFC using resting state fMRI: functional connectivity-based parcellation method. Neuroimage. 49:2375–2386.

Lashkari D, Vul E, Kanwisher N, Golland P. 2010. Discovering structure in the space of fMRI selectivity profiles. Neuroimage. 50:1085–1098.

Lee JD, Park HJ, Park ES, Oh MK, Park B, Rha DW, Cho SR, Kim EY, Park JY, Kim CH, et al. 2011. Motor pathway injury in patients with periventricular leucomalacia and spastic diplegia. Brain. 134:1199–1210.

Minagawa-Kawai Y, Matsuoka S, Dan I, Naoi N, Nakamura K, Kojima S. 2009. Prefrontal activation associated with social attachment: facial-emotion recognition in mothers and infants. Cereb Cortex. 19:284–292.

Mumford JA, Horvath S, Oldham MC, Langfelder P, Geschwind DH, Poldrack RA. 2010. Detecting network modules in fMRI time series: a weighted network analysis approach. Neuroimage. 52:1465–1476.

Phillips NK, Hammen CL, Brennan PA, Najman JM, Bor W. 2005. Early adversity and the prospective prediction of depressive and anxiety disorders in adolescents. J Abnorm Child Psychol. 33:13–24.

Power JD, Cohen AL, Nelson SM, Wig GS, Barnes KA, Church JA, Vogel AC, Laumann TO, Miezin FM, Schlaggar BL, et al. 2011. Functional network organization of the human brain. Neuron. 72:665–678.

Power JD, Barnes KA, Snyder AZ, Schlaggar BL, Petersen SE. 2012. Spurious but systematic correlations in functional connectivity MRI networks arise from subject motion. Neuroimage. 59:2142–2154.

Rubinov M, Sporns O. 2010. Complex network measures of brain connectivity: uses and interpretations. Neuroimage. 52:1059–1069.

Salzwedel AP, Grewen KM, Goldman BD, Gao W. 2016. Thalamocortical functional connectivity and behavioral disruptions in neonates with prenatal cocaine exposure. Neurotoxicol Teratol. 56:16–25.

Salzwedel AP, Grewen KM, Vachet C, Gerig G, Lin W, Gao W. 2015. Prenatal drug exposure affects neonatal brain functional connectivity. J Neurosci. 35:5860–5869.

Scharoun SM, Bryden PJ. 2014. Hand preference, performance abilities, and hand selection in children. Front Psychol. 5:82.

Shen X, Papademetris X, Constable RT. 2010. Graph-theory based parcellation of functional subunits in the brain from resting-state fMRI data. Neuroimage. 50:1027–1035.

Shi F, Yap PT, Wu G, Jia H, Gilmore JH, Lin W, Shen D. 2011. Infant brain atlases from neonates to 1- and 2-year-olds. PLoS One. 6:e18746.

Shi J, Malik J. 2000. Normalized cuts and image segmentation. IEEE Trans Pattern Anal Mach Intell. 22:888–905.

Singer LT, Hawkins S, Huang J, Davillier M, Baley J. 2001. Developmental outcomes and environmental correlates of very low birthweight, cocaine-exposed infants. Early Hum Dev. 64:91–103.

Smith SM, Miller KL, Salimi-Khorshidi G, Webster M, Beckmann CF, Nichols TE, Ramsey JD, Woolrich MW. 2011. Network modelling methods for FMRI. Neuroimage. 54:875–891.

Smyser CD, Inder TE, Shimony JS, Hill JE, Degnan AJ, Snyder AZ, Neil JJ. 2010. Longitudinal analysis of neural network development in preterm infants. Cereb Cortex. 20:2852–2862.

Tau GZ, Peterson BS. 2010. Normal development of brain circuits. Neuropsychopharmacology. 35:147–168.

Zhang J, Tuo X, Yuan Z, Liao W, Chen H. 2011. Analysis of FMRI data using an integrated principal component analysis and supervised affinity propagation clustering approach. IEEE Trans Biomed Eng. 58:3184–3196.